Applied Catalysis B: Environmental 150–151 (2014) 238–248

Contents lists available at ScienceDirect

Applied Catalysis B: Environmental

journal homepage: www.elsevier.com/locate/apcatb

Hydroprocessing of waste cooking oil over a dispersed nano catalyst: Kinetics study and temperature effect

Haiping Zhang[a], Hongfei Lin[a], Weizhi Wang[a], Ying Zheng[a,*], Peijun Hu[b]

[a] Department of Chemical Engineering, University of New Brunswick, 15 Dineen Drive, Fredericton, NB, Canada E3B 5A3
[b] School of Chemistry and Chemical Engineering, Queen's University Belfast, Stranmillis Road, Belfast, Northern Ireland, United Kingdom BT9 5AG

ARTICLE INFO

Article history:
Received 2 May 2013
Received in revised form 31 October 2013
Accepted 6 December 2013
Available online 14 December 2013

Keywords:
Unsupported catalyst
CoMoS
Waste cooking oil
Hydroprocessing
Kinetics

ABSTRACT

The kinetics of hydrodeoxygenation of waste cooking oil (WCO) is investigated with unsupported CoMoS catalysts. A kinetic model is established and a comprehensive analysis of each reaction pathway is carried out. The results show that hydrodecarbonylation/decarboxylation (HDC) routes are the predominant reaction pathways in the elimination of oxygen, with the rate constant three times as high as that of hydrodeoxygenation (HDO). However, the HDC activity of the CoMoS catalyst deactivates due to gradual loss of sulfur from the catalyst. HDO process is insensitive to the sulfur deficiency. The kinetic modeling shows that direct hydrodecarbonylation of fatty acids dominates the HDC routes and, in the HDO route, fatty acids are transferred to aldehydes/alcohols and then to C_{18} hydrocarbons, a final product, and the reduction of acids is the rate limiting step. The HDO route via alcohols is dominant over aldehydes due to a significantly higher reaction rate constant. The difference of C_{18}/C_{17} ratio in unsupported and supported catalysts show that a support with Lewis acid sites may play an important role in the selectivity for the hydrodeoxygenation pathways and promoting the final product quality.

1. Introduction

Waste cooking oil (WCO) is accepted as a second generation resource for biofuel production [1–3]. Its main component, triglycerides, can be easily converted to combustible biofuel. However, due to the high oxygen content in triglycerides, the final products containing oxygen e.g. FAME, lead to poor storage stability, lower blending degree with petroleum diesel, and even cause engine compatibility issues [4,5]. Therefore, production of oxygen-free biodiesel is necessary to overcome these drawbacks and hydrotreating is a promising technique [6,7].

In order to produce oxygen-free biodiesel, many efforts have been made to study the mechanism of deoxygenation process. Previous works summarized that the deoxygenation process of triglycerides primarily occurs through two parallel paths: hydrodeoxygenation (HDO) route and hydro decarbonylation/decarboxylation (HDC) route. A main difference between the two pathways is the carbon yield in the final products: hydro decarbonylation/decarboxylation route leads to hydrocarbons with one carbon number lower than the feed oxygenates due to formation of CO or CO_2, while hydrodeoxygenation product maintains the same carbon number [8–12]. Carboxylic acids, aldehydes, and alcohols are identified as the major intermediates, and their generation and consumption rates determine the total deoxygenation capability and selectivity [5,13,14]. Therefore, the real-time concentrations (RTC) of these intermediates are of great importance when studying deoxygenation process kinetics. Presently, most mechanism studies are focused on the model oils, which generally contain only one or few components [5,13–16]. This may lead to misunderstanding of the actual deoxygenation process on real WCO feed as the RTC could be altered without considering the influence of the complex feedstock compositions [8].

Another factor that may influence the oxygen removal is the support material of catalysts. Currently, commercial supported catalysts are widely employed in hydrotreatment of vegetable oils. The hydrotreating performance may involve the contribution of support material, and the catalyst support, alumina, alone has catalytic activity in hydrotreating reactions due to the Lewis acid site [16]. Centeno et al. investigated the effects of different support materials on the reaction pathways and product distribution. The report showed that acidity of support materials can influence the formation of catalysts' active sites for hydrogenation and decarboxylation of diethylsebacate [17]. Use of unsupported catalysts is a good alternative to investigate the activity of the active phase without involvement of support materials. In addition, unsupported catalyst presents minimal mass transfer resistance so as to minimize secondary effects, such as adsorption, re-adsorption and diffusion. A recently published work reported that the hydrodeoxygenation reaction of guaiacol (2-methoxyphenol) over unsupported and

* Corresponding author. Tel.: +1 506 447 3329.
E-mail address: yzheng@unb.ca (Y. Zheng).

0926-3373/$ – see front matter © 2014 Elsevier B.V. All rights reserved.
http://dx.doi.org/10.1016/j.apcatb.2013.12.006

Table 1
Comparison of hydrotreating results with and without catalyst at 375 °C.

	Blank (without catalyst)		With catalyst	
Hydrotreating time	1 h	8 h	1 h	8 h
Oxygen conversion (%)	2.94	9.62	41.72	98.31
Glycerides conversion (%)	8.93	35.16	90.90	99.87

supported MoS_2 and CoMoS catalysts [18]. Guaiacol was used to represent pyrolysis oil of ligno-cellulosic biomass. However, limited reports were on the application of unsupported catalysts in the hydrodeoxygenation of triglyceride-type bio-oil.

In this work, a comprehensive kinetics analysis was carried out to understand the deoxygenation process using waste cooking oil and unsupported CoMoS. Reaction mechanisms and catalyst deactivation were investigated using kinetic modeling based on a proposed reaction network. The calculated rate constants indicate dominant reactions and rate-limiting steps in a series of parallel and consecutive reactions. Other reactions including hydrocracking, polymerization, hydrogenation, and cyclization were also studied as well as the reaction temperature effect. The comprehensive analysis of deoxygenation process would provide valuable information on the mechanism study of vegetable oil type feedstock with unsupported catalysts.

2. Experimental

2.1. Catalyst synthesis

Unsupported catalyst CoMoS was synthesized using a hydrothermal method with MoO_3 (purchased from the STEM Scientific), $Na_2S{\cdot}9H_2O$ and $Co(NO_3)_2{\cdot}6H_2O$ (from the Fisher Scientific) as precursors. The precursors were dissolved in deionized water before introducing them into an autoclave reactor. The hydrothermal reaction lasted for 2 h at 320 °C. The detailed synthesis procedure is referred to Zhang et al. [19].

2.2. Hydrotreating process

A batch reactor (Autoclave Engineers Inc.) was used in this study, 0.6 g of unsupported CoMoS catalyst and 120 g of waste cooking oil (WCO) were added to the reactor, making the catalyst-to-oil ratio 1:200 by weight. The reactor was heated to pre-set temperatures (300–375 °C) and kept for 8 h under a stirring speed of 1000 rpm. The pressure was maintained at 1300 psi at the reaction temperatures. Liquid samples were taken at different time intervals during the reaction. The gaseous products were collected when the reaction was complete and the reactor was cooled down to room temperature. In this experiment, the internal and external mass transfer for the catalyst was assumed to be negligible, since nano-sized dispersed catalyst powders were applied [20]. For comparison purpose, a blank experiment (without catalyst) was carried out under the same hydrotreating condition at 375 °C. Table 1 shows low glycerides and oxygen conversions compared to the situation with catalyst. Therefore, the thermal effect was not considered in the kinetics studies.

2.3. Characterization

Transmission electron microscopy (TEM) was performed on an electron microscope (JEOL 2011 STEM, JEOL Ltd., Tokyo, Japan) operating at 200 keV. The catalyst powder was ultrasonically dispersed in ethanol and deposited on a carbon-coated copper grid, then vacuum-dried for 12 h before analysis. The length and layer numbers of CoMoS crystalline were determined using image analysis software and the average was calculated based on at least 100 CoMoS measures from various particles. Selected area electron diffraction (SAD) pattern was used for the determination of catalyst crystal structure. The Co/(Co + Mo) ratio of the catalyst was estimated by energy dispersive X-ray emission (EDX) coupled with TEM.

The fatty acids of WCO were analyzed following the procedure described by Simaeck et al. [21]. The oil sample was added to a flask containing methanolic NaOH solution and heated until all WCO was completely dissolved. By introducing BF_3-methanol and boiling for 2 min complete esterification occurred. Petroleum ether and saturated NaCl solutions were then added to extract and separate the organic components. The resultant fatty acid methyl esters appeared in the top petroleum ether layer and were analyzed using a gas chromatography–mass spectrometry (Shimadzu GCMS-QP5000) with a weak-polarity column (Agilent J&W HP-5).

The components in the oil products were identified by GC–MS (Shimadzu GCMS-QP5000) and quantified using gas chromatography (Varian 450) equipped with a hydrogen flame ionization detector. A non-polarity capillary column Agilent J&W VF-1ms was used to quantify hydrocarbons. The free fatty acids were analyzed using both gas chromatography (Shimadzu GC-17A) and titration (ZD-2A Automatic potentiometric titrator, Saegmoter Company, Shanghai, China) according to ASTM-D664. The content of intermediate alcohols and aldehydes was estimated by the peak area (MS%) and response factor to *n*-heptadecane of 1.3 and 1.4, respectively [22]. The unreacted triglycerides were derived from the oxygen content.

The original WCO and the upgraded products were analyzed using a Fourier transform infrared spectrometer (FTIR) (Nicolet 6700, Thermo Scientific, US). The spectra were collected for 32 scans at a resolution of 4 cm^{-1} in the range of 400–4000 cm^{-1}. ^1H nuclear magnetic resonance (NMR) spectra were recorded with a high-field multinuclear Agilent UNITY INOVA NMR spectrometer (Varian Unity 400) under standard acquisition conditions. The operating frequencies were 300 MHz; D-chloroform was used as solvent.

The elemental analysis for WCO and upgraded products were conducted on CHNS-O 932 elemental analyzer (LECO Corporation, MI, US). The oxygen content was calculated from the balance. The minimum measurability is 10 ppm for carbon and 100 ppm for hydrogen on the basis of a normal sample load (i.e. 2 mg). The density of the liquid oil was measured using a portable density meter (DMA 35N, Anton Paar GmbH, Graz, Austria).

CO and CO_2 generated during hydrotreating were analyzed using a gas chromatography Varian 3400 equipped with a thermal conductivity detector. Hydrocarbons, C1–C6, were examined using a Shimadzu GC-17A equipped with a flame ionization detector.

3. Results and discussion

3.1. Unsupported catalysts

The TEM images shown in Fig. 1 illustrate a well dispersed (a) and layered crystalline structure (b) of unsupported nano-sized CoMoS catalyst. The average crystalline size was calculated by Eqs. (1) and (2), where L, N and n stand for slab length, number of layers in each crystal, and the total number of crystalline measured, respectively. The statistic results show that the catalysts have an average layer number of 3 and an average slab length of 7.8 nm. According to Rim and Edge theory, Co decorated at the edge of MoS_2 [23,24]. EDX results show the average Co/(Co + Mo) atomic ratio is 25%. The well-dispersed MoS_2 slabs provide abundant active sites for hydrodeoxygenation. The MoS_2 crystalline structure was also confirmed by electron diffraction spectra on the selected area

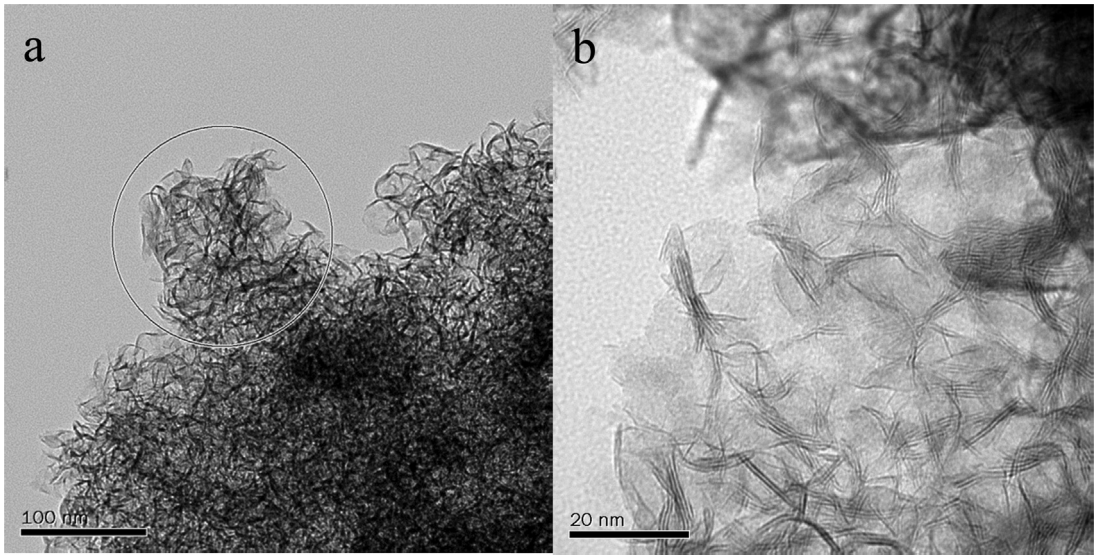

Fig. 1. TEM images of unsupported CoMoS catalyst.

shown in Fig. 2, where the typical MoS_2 diffraction rings can be observed. The blurry rings indicated nanosized crystalline. The *d*-values of CoMoS are essentially the same as MoS_2 synthesized at the same condition.

$$\text{Average layer number } \bar{N} = \frac{\sum_{i=1,2\ldots n} N_i}{n} \quad (1)$$

$$\text{Average slab length } \bar{L} = \frac{\sum_{i=1,2\ldots n} L_i N_i}{\sum_{i=1,2\ldots n} N_i} \quad (2)$$

3.2. Overall description of WCO and hydrotreated product

The composition of fatty acid in WCO was determined by GC–MS (Table 2). Most fatty acids detected are present in the form of triglycerides, in addition that the total acid number (TAN) of WCO is low (0.65). The triglycerides structure is identified by FTIR and ^{1}H-NMR spectra, with the presence of the large peaks of esters at 1740 and 1163 cm^{-1} and peaks 2,3,5 and 7 for protons related to ester and carboxylic groups [25], respectively (Fig. 3 and Fig. 4). In Table 2, it is noted that the fatty acids having even number of

Table 2
Composition of fatty acids in WCO.

Fatty acids (*n*:*m*)*	≤14:0	16:0	18:0	18:1	18:2	≥20:0
Content (%wt)	0.3	5.8	1.3	73.9	17.6	1.1

* *n*: number of carbon atoms in fatty acids; *m*: number of C=C double bonds in fatty acids e.g. 18:1: a fatty acid with 18 carbon atoms and one C=C double bond

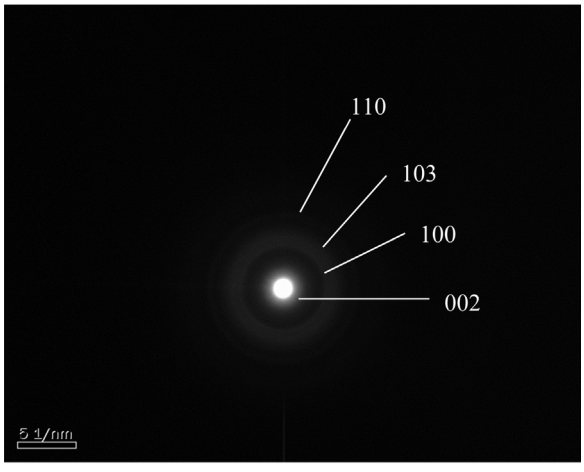

Fig. 2. Electron diffraction spectra of unsupported CoMoS catalyst (from the circle in Fig. 1).

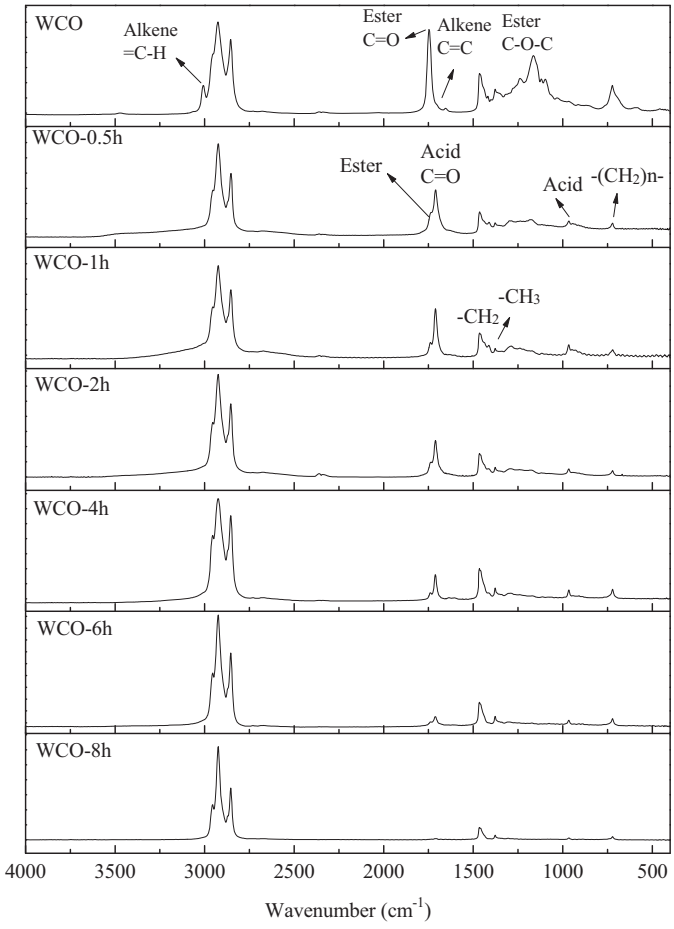

Fig. 3. FTIR spectra of original and hydrotreated WCO (375 °C).

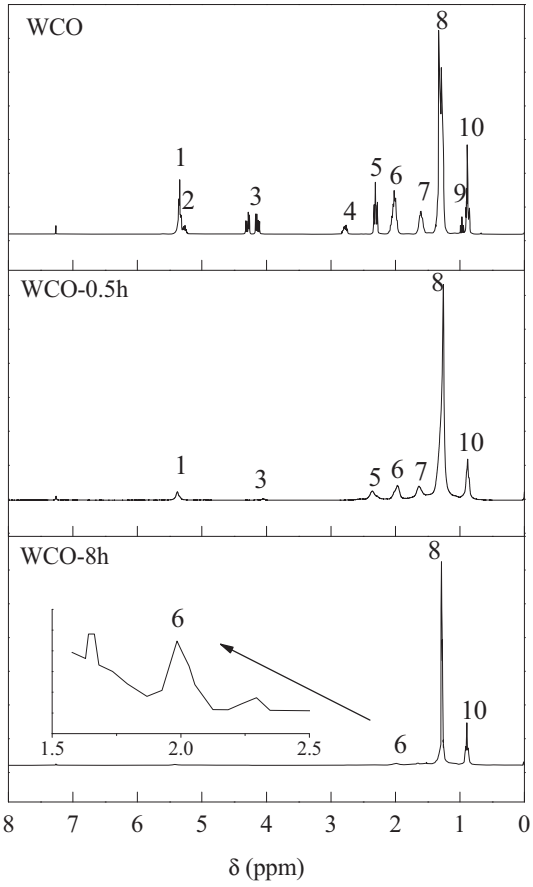

Fig. 4. H-NMR spectra for original and hydrotreated WCO (375 °C).
Peaks 1–10 (**H** in bold): 1. C**H**=CH, 2. C**H**–OCOR, 3. C$\mathbf{H}_2$–OCOR, 4. CH=CH–C$\mathbf{H}_2$–CH=CH, 5. C$\mathbf{H}_2$–COOH, 6. C$\mathbf{H}_2$–CH=CH, 7. C$\mathbf{H}_2$–CH_2COOH, 8. $(\mathbf{CH_2})_n$, 9. CH=CH–CH_2–C$\mathbf{H}_3$, 10. $CH_2CH_2CH_2$–C$\mathbf{H}_3$ [25]

carbon atoms exist in WCO and over 90 wt% are C_{18} fatty acids, most of which are unsaturated with one or two C=C double bonds.

The waste cooking oil was hydrotreated in a batch autoclave reactor, allowing sampling at different time intervals during the hydrotreating reaction. Due to small amounts of sampling (1.0 g/sample), the effect of sampling is reasonably assumed to be negligible to the hydrotreating reaction. The reactor was oxidized before each hydrotreating test in order to minimize the influence of the reactor wall.

The variation of glycerides and fatty acids along with reaction is identified by the FTIR and NMR as shown in Figs. 3 and 4. The sharp FTIR peak centered at 1740 cm^{-1} – representing esters in WCO – noticeably diminishes and shifts to 1711 cm^{-1}, a characteristic peak of fatty acids, after half an hour hydrotreatment. The peaks centered at 1163 cm^{-1} standing for C–O–C of esters also dramatically decreases (Fig. 3). The peaks at 1711 and 965 cm^{-1} characterizing the absorption of fatty acids weaken with the reaction until disappearing after 8 h of hydrotreating. In NMR spectra, peaks 2 and 3 representing protons in ester group of triglycerides vanish in half an hour and peaks 5 and 7 assigned to the protons on the acyl chains associated with carboxylic group diminish and finally disappear at 8 h. These variations along the reaction process are further illustrated in Fig. 5. It is seen that triglycerides are quickly decomposed to fatty acids in the initial reaction, and then the decomposition rate slows down gradually. Within the first half an hour of the reaction, more than 70% of triglycerides are converted to fatty acids. Correspondingly, the acid number of the hydrotreated products increase abruptly from 0.65 of the feed WCO to 110 mg KOH/g oil when a majority of triglycerides are decomposed, this value then

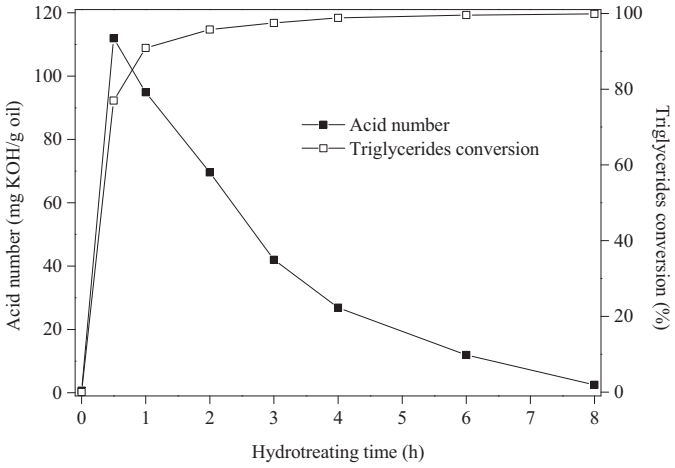

Fig. 5. Acid number and triglycerides conversion (375 °C).

steadily declines to a minimum at the end of the reaction (Fig. 5). This confirms that fatty acids are an intermediate product of de-esterification of triglycerides. Fatty acids are the main cause of the acidity of the WCO and hydrotreated products; this finding is consistent with the literature [11].

The WCO contains even-numbered-carbon-atom acids only as discussed previously and shown in Table 2. After hydrotreatment, both odd- and even-numbered-carbon-atom hydrocarbons can be observed in the liquid hydrotreated products. Fig. 6 shows the distribution of hydrocarbons in the liquid products at different hydrotreating times. Hydrocarbons with odd numbered carbon atoms appear at higher concentrations than the even numbered carbon atom counterparts. In particular, hydrocarbons, C_{17}, reach approximately 40% in the final liquid product. Generation of odd-numbered-carbon-atom hydrocarbons suggests the existence of decarbonization reaction.

In comparison with the feed WCO (Table 2), the hydrotreated products have a wider range of hydrocarbons and the distribution becomes more diversified with hydrotreating time (Fig. 6). Hydrocarbons lighter than C_{14} increase from approximate 0.3 wt% initially to 2.2 wt% in the liquid product after only half an hour of hydrotreatment. A detailed comparison was made between WCO feed and hydrotreated WCO at the completion of the reaction (Fig. 7). A decrease of C_{17} and C_{18} is clearly seen and a corresponding increase of other components can also be seen. 27% of C_{17} and C_{18} is converted to lighter or heavier hydrocarbons, of which 11% falls in

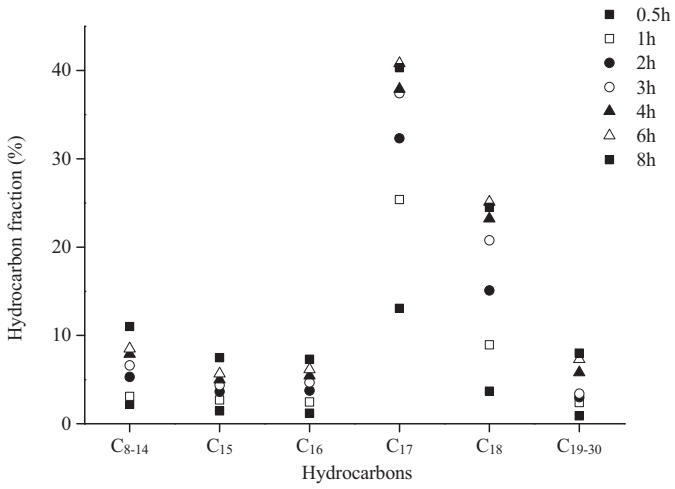

Fig. 6. Hydrocarbon distribution at different hydrotreating times (375 °C).

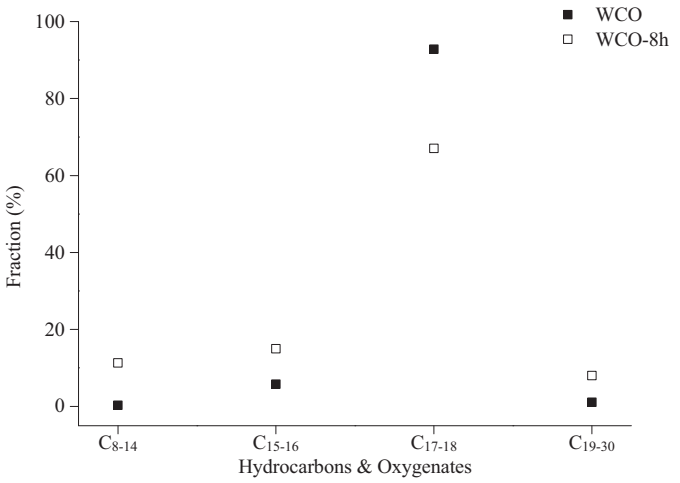

Fig. 7. Comparison of different carbon-number compounds (hydrocarbons and oxygenates).
WCO: triglycerides, WCO-8 h: hydrocarbon and fatty acids (375 °C)

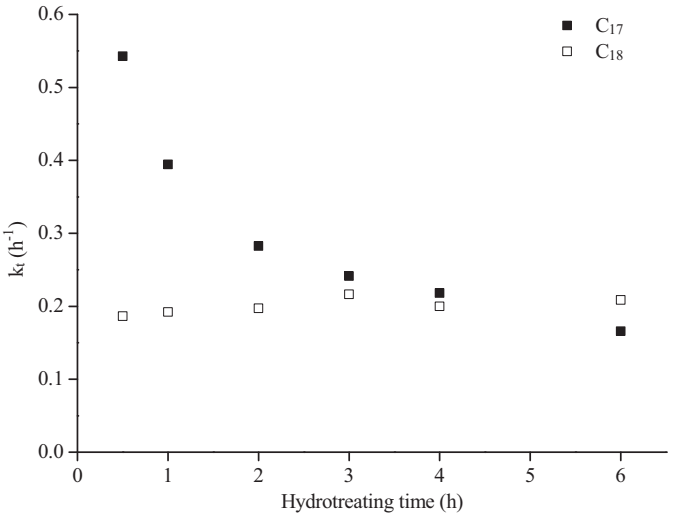

Fig. 9. Instant rate constants (k_t) variation during the reaction (375 °C).

the range of C_8 and C_{14}, 9% between C_{15} and C_{16}, and 7% between C_{19} and C_{30}. The lighter alkanes are derived due to hydrocracking, whereas the long-chain hydrocarbons are the products of polymerization.

The hydrogenation reaction can be evidenced by acids distribution. The feed WCO contains high contents of unsaturated fatty acids including 17.6% linoleic (18:2) and 73.9% linolenic acids (18:1) (Table 2). In Fig. 8, free $C_{18}^{==}$ (18:2) fatty acids are not detected in the hydrotreated products, indicating all the linoleic acids have been hydrogenated to linolenic ($C_{18}^{=}$) or saturated acids (C_{18}) before hydrolysis of triglycerides. In addition, linolenic acids also decrease dramatically with reaction time from 37% at 0.5 h to 10% at 2 h. Saturated acids (C_{18}) increased from 1.3% in the feed to the highest value 19% at 2 h. The increment of saturated acids is attributed to the saturation of linoleic and linolenic acids. The hydrogenation reaction can be further evidenced by the FTIR and H-NMR spectra shown in Fig. 3 and Fig. 4. Disappearance of the FTIR peaks at 3007.3 cm^{-1} (assigned to =C–H) and at 1654 cm^{-1} (assigned to C=C) demonstrates hydrogenation of double bonds (Fig. 3). Similarly, saturation of double bonds is also seen from the decreased or vanished peaks of 1, 4, 6 and 9 in NMR spectra. The disappearance of peak 4, specifically, after 30 min implies the quick saturation of linoleic compounds (Fig. 4). Note that a small peak at chemical shift of 2.00 observed in Fig. 4 suggests the presence of unsaturated acyl chain after 8 h, indicating an incomplete saturation. In addition, –CH is not detected in the product suggests a nearly pure, straight chain structure (Fig. 4).

Fig. 9 shows the instant rate constants of the generation of C_{17} and C_{18}. Eq. (3) defines the instant rate constants at reaction time t. It is noticed that the rate constant k_t of C_{17} decreases while the rate constant for C_{18} is mainly kept constant during the reaction. It indicates that the catalyst deactivates over the HDC activity only.

$$\frac{dC_{Cn,t}}{dt} = k_t c_{a,t} \quad (3)$$

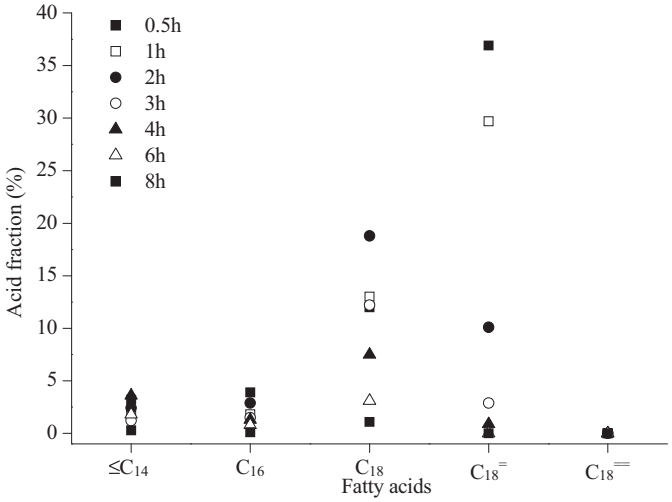

Fig. 8. Fatty acids distribution at different hydrotreating times (375 °C).
C_{14}, C_{16}, C_{18}: saturated fatty acids; $C_{18}^{=}$: with one C=C double bond; $C_{18}^{==}$: with two C=C double bonds

3.3. Kinetic modeling

3.3.1. Sketched reaction routes and deactivation of catalyst

To understand the reaction pathways of oxygen removal process, a kinetic model of hydrotreatment is proposed on the basis of the findings described in Section 3.2. The simplified hydrotreating pathways are presented in Scheme 1. Decomposition of glycerides to fatty acids is a very fast reaction and its rate constant is denoted as k_1. Glycerol, a by-product of the decomposition, can be quickly converted to propane and propene over the catalyst, which is confirmed by Fig. 10. Thus, decomposition of glycerides to fatty acids is assumed to be an irreversible reaction. Fatty acids are then further transferred to hydrocarbons through different routes since CO, CO_2 and H_2O are detected in gas and liquid products. Given sufficient hydrogen gas, the reaction that fatty acids are hydrodeoxygenated to C_{18} is assumed to be pseudo-first-order-kinetics. Its reverse reaction is neglected due to the fact that low oxygenation activity of

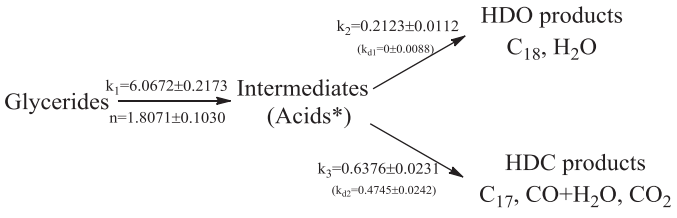

* A small amount of other oxygenate intermediates are detected.

Scheme 1. Simplified reaction pathways.

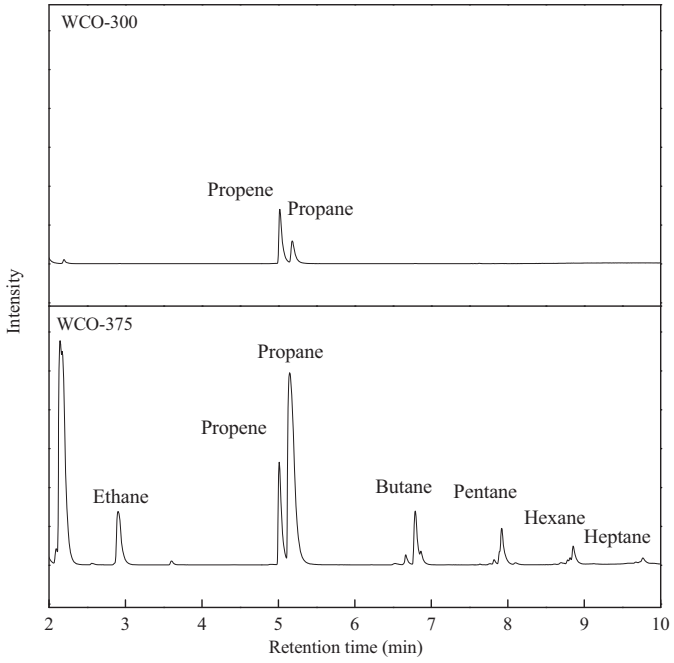

Fig. 10. Organic gas analysis of hydrotreated WCO (8 h).

MoS_2 and sufficient hydrogen atmosphere. The HDC reaction is also considered as an irreversible reaction to be consistent with the previous reports [13,26]. The rate constants for HDO and HDC products are denoted as k_2 and k_3, respectively. Deactivation of catalyst is taken into account for both HDO and HDC reactions. A commonly used second-order decay law is applied on both routes. The corresponding specific decay constants are denoted as k_{d1} and k_{d2}.

Eqs. (4)–(9) show mass balance, reaction kinetics, and catalyst deactivation. The Runge–Kutta method and trust-region-reflective optimization algorithm with least squares as objective function are applied, and the confidence intervals of the rate constants are estimated under 0.95 confidence level based on an asymptotic normal distribution for the parameter estimate. The resulted k values with their confidence intervals are shown at their corresponding reaction routes. For an instance, rate constant k is denoted as $k = m \pm \Delta$, where m is the estimated value of k and Δ is the upper bound of the confidence interval, that is, 95% possibility of the true k value falls in between $m - \Delta$ and $m + \Delta$. It is seen that the estimation of rate constants is reliable due to low deviations of the estimates.

$$\frac{dc_g}{dt} = -k_1 c_g^n \tag{4}$$

$$\frac{dc_a}{dt} = k_1 c_g^n - a_1 k_2 c_a - a_2 k_3 c_a \tag{5}$$

$$\frac{dc_{C_{18}}}{dt} = a_1 k_2 c_a \tag{6}$$

$$\frac{dc_{C_{17}}}{dt} = a_2 k_3 C_a \tag{7}$$

$$\frac{da_1}{dt} = k_{d1} a_1^2 \tag{8}$$

$$\frac{da_2}{dt} = k_{d2} a_2^2 \tag{9}$$

where c_g represents the mass fraction of total glycerides (mono-, di- tri-); c_a stands for the total concentration of intermediate fatty acids; $c_{C_{18}}$ and $c_{C_{17}}$ are the total mass fraction of HDO and HDC produced hydrocarbons, respectively. a_1 and a_2 showing the catalyst activities of HDO and HDC, are defined as the ratio of a reaction rate at $t = t$ to the initial reaction rate at $t = 0$. Catalyst deactivation occurs when the value of a is less than 1.

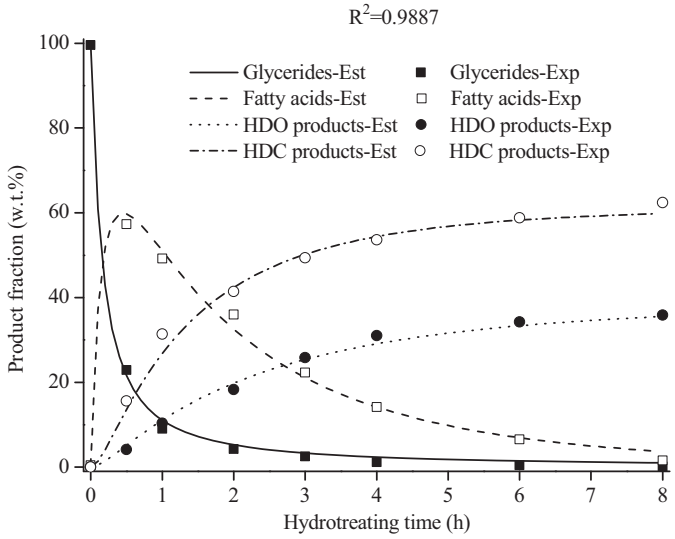

Fig. 11. Comparison of experimental data and modeling results of sketched reaction routes (375 °C).
Est: estimates; Exp: experimental data.

Comparison of the estimated results and the experimental data is shown in Fig. 11. R^2 is calculated by Eq. (10), where c_{exp} and c_{est} stand for the experimental data and estimated values, respectively. A good agreement can be seen.

$$R^2 = 1 - \frac{\left(C_{exp} - C_{est}\right)^2}{\left(C_{exp} - \bar{C}_{exp}\right)^2} \tag{10}$$

From Scheme 1, one may note that HDC reaction is the predominant reaction pathway because the rate constant of HDC is three times as high as that of HDO. The total deactivation rate (TDR) of catalysts can be revealed by the sum of k_{d1} and k_{d2}, which leads to a remarkable 80% activity lost by the end of the reaction. A possible reason may be gradual loss of sulfur on the catalyst surface, which is evident by the significant increase of sulfur content in the hydrotreated products (140 ppm comparing to the feed 30 ppm, about 3% of the catalyst sulfur). Comparing k_{d1} to k_{d2} suggests that the catalyst deactivation is primarily contributed by the HDC reaction ($k_{d2} = 0.4745$) while the HDO activity is well maintained during the entire reaction course ($k_{d1} = 0$). It indicates a different reaction mechanism between the HDO and the HDC over catalyst CoMoS. HDO takes place at the active sites that are unsaturated and oxygen is removed by the sulfur vacancy on the catalyst surface. HDC involves the steps occurring on the sulfur saturated sites. Sulfur is continuously lost during the reaction, which lowers the sulfur saturated sites and thus reaction rates of HDC are reduced significantly. On the other hand, the activity of HDO is retained due to maintenance of a similar amount of active sites, which is a combined result of new vacancy sites created by hydrogen reduction and loss of active sites due to oxygen occupation. This is consistent with the report given by D. Kubicka and J. Horacek [27].

3.3.2. *Detailed kinetics for the oxygen elimination process*

Possible reaction routes for the deoxygenation of C_{18} fatty acid are proposed in Diagram 1. Prior to the simulation, significance of each reaction pathway is equally treated and dominant reaction pathways are determined by the simulation results. The

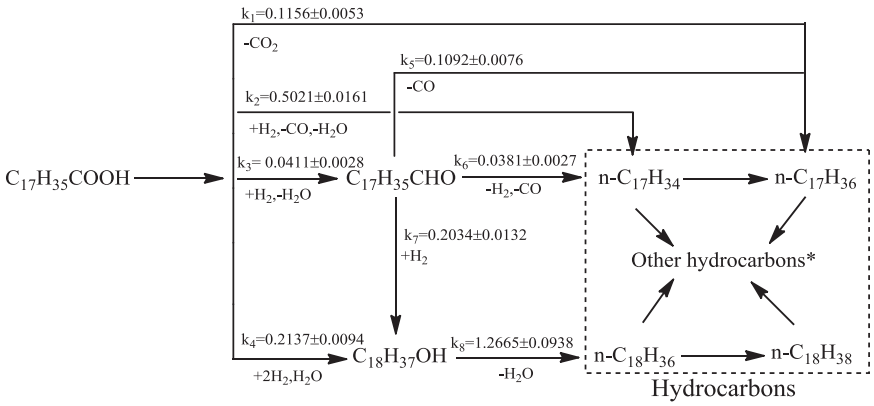

*Other hydrocarbons include products from hydrocracking, polymerization, and cyclization.
The reactant hydrogen and by-products are listed under the arrows.

Diagram 1. Proposed reaction routes for the consumption of carboxylic acid.

Runge–Kutta method is used in the simulation, the same algorithms used for derivation of Scheme 1. Confidence intervals for each *k* are estimated at confidence level of 0.95.

In Diagram 1, C_{18} and C_{17} hydrocarbons are the two main components of the final liquid products, while aldehydes and alcohols are intermediates. C_{17} hydrocarbons are the products of HDC reactions through different reaction pathways. Saturated hydrocarbon C_{17} can either be produced from fatty acids through decarboxylation with by-product of CO_2 [16] or from aldehydes via decarbonylation with CO as by-product [13]. Unsaturated C_{17} is derived directly from fatty acids with by-products of H_2O and CO [10] or from aldehydes through decarbonylation reaction with by-products of CO and H_2 [15]. The C_{18} hydrocarbons are obtained via hydrodeoxygenation, primarily from alcohols with H_2O as by-product [28,29]. For intermediates, aldehydes are reduced from fatty acids, and alcohols can either be formed by further reduction of aldehydes or directly from fatty acids [12,30]. As seen in Diagram 1, deviations of the estimates are low, indicating reliable results. The estimated results are compared to the experimental data as shown in Fig. 12.

The simulation results suggest that direct decarbonylation is a main pathway, due to the highest rate constant (k_2 = 0.5021). k_1 (0.1156) is significantly lower than k_2, indicating that direct decarbonylation primarily produces C_{17}-alkenes and CO. The final product, C_{17}-alkanes is resulted from the hydrogenation of C_{17}-alkenes. This can be evidenced by the ratio CO to CO_2 of 10:1. This finding supports with previous reports that hydrogen enhanced decarbonylation selectivity over decarboxylation [31].

Reduction of fatty acids is carried out through a series of reactions. The simulation result indicates that direct deoxygenation of acids to produce alcohol is a key pathway since k_4 (0.2137) is approximately 5 folds of k_3 (0.0411). This is consistent with the experimental results shown in Fig. 12 where the concentration of alcohol is much higher than aldehydes. A similar mechanism was demonstrated with metal ion/oxygen vacancy created in the reducible oxide in the presence of platinum [32]. However, there is an argument that the formation of alcohol is essentially correlated to decomposition of aldehydes [13]. In this work, catalyst CoMoS is used. The unsaturated sulfur vacancies on CoMoS catalysts have a strong capability to capture oxygen atoms from carbon–oxygen double bonds and the double bonds can be fully broken to form alcohols. It supports the simulation result. With a high dehydration ability (k_8, 1.2665), the reduction of fatty acids is the limiting step of HDO pathway.

After the kinetics analysis, the main deoxygenation reaction routes are summarized in Scheme 2. Three main routes are identified, direct decarbonylation and decarboxylation from fatty acids and hydrodeoxygenation to generate alcohols. The deoxygenation rate constants follow in the order of decarbonylation > hydrodeoxygenation > decarboxylation.

3.3.3. Hydrogenation, hydrocracking, polymerization and cyclization

Besides the oxygen elimination reactions, hydrogenation also occurs so that the unsaturated bonds become saturated. The degree of hydrogenation is revealed by degree of unsaturation, i.e. the

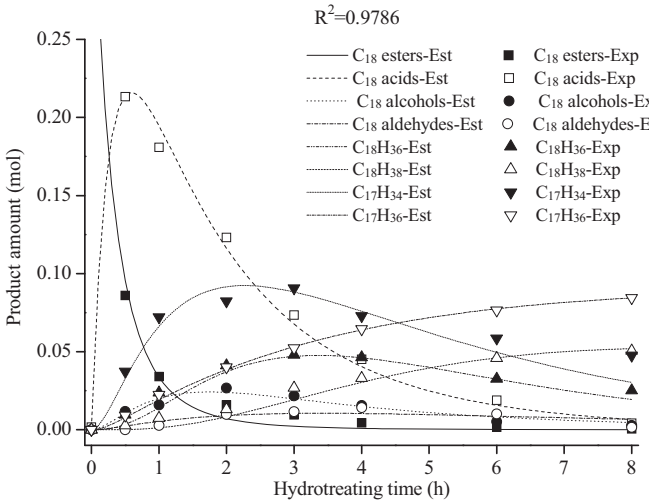

Fig. 12. Comparison of experimental data and modeling results of detailed kinetics (375 °C).
Est: estimates; Exp: experimental data.

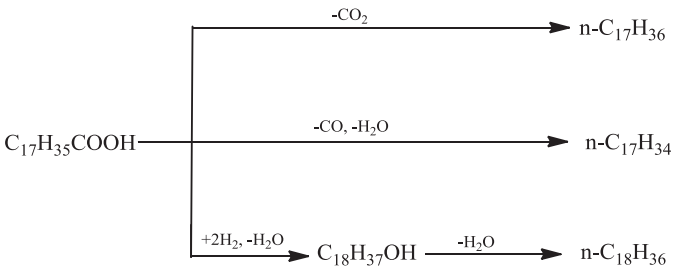

Scheme 2. Main deoxygenation reaction routes.

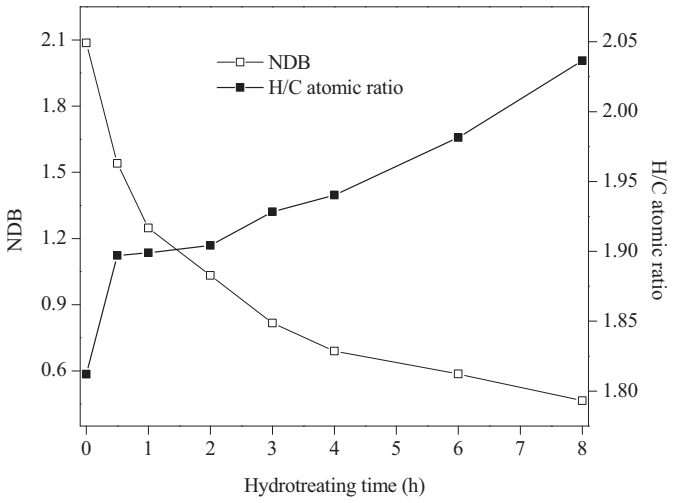

Fig. 13. The number of double bonds (NDB) and H/C atomic ratio (375 °C).

number of double bonds (NDB) in the products. For component i, NDB_i can be calculated by Eq. (11) [33], in which C is the number of carbon and H is the number of hydrogen. The total NDB is expressed as the sum of NDB of each component i based on 1 mole of feed oil (Eq. (12)). Fig. 13 shows the number of double bonds (NDB) and H/C atomic ratio varying with the reaction. It is seen that the NDB decreases with increasing reaction time, indicating a continuous saturation of double bonds. A quick drop from 2.1 to 1.5 occurs in the first half an hour and then the decrease slows down. A corresponding observation is shown for the variation of H/C atomic ratio. The H/C ratio increases from 1.81 to 1.89 in the first 0.5 h and reaches 2.04 after 8 h of reaction. The dramatic decrease of NDB in the beginning is caused by a rapid hydrogenation of the double bonds of unsaturated fatty acids. The proceeding decrease may be attributed by saturation of the C=C generated during the reaction.

$$NDB_i = C + 1 - \frac{H}{2} \quad i: \text{hydrocarbons and oxygenates} \tag{11}$$

$$NDB = \frac{\sum_{i=1,2\ldots n} NDB_i \times n_i}{n_{tot,o}} \quad n_{tot,o}: \text{initial feed moles} \tag{12}$$

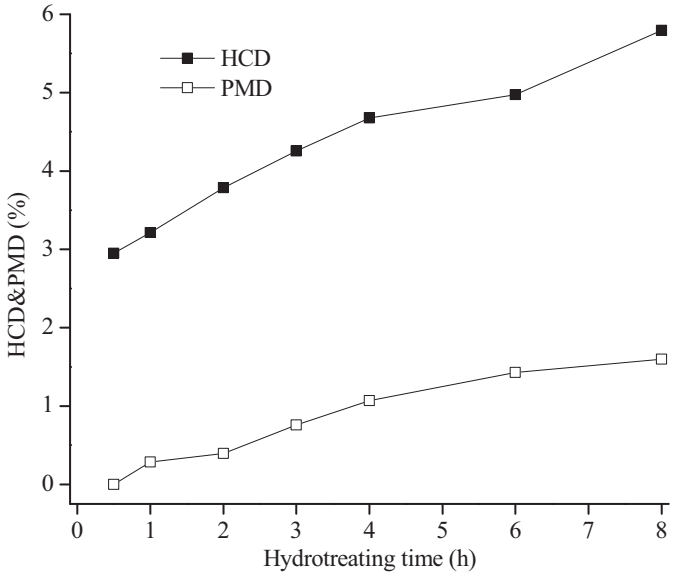

Fig. 14. Hydrocracking and polymerization degree (HCD&PMD) (375 °C).

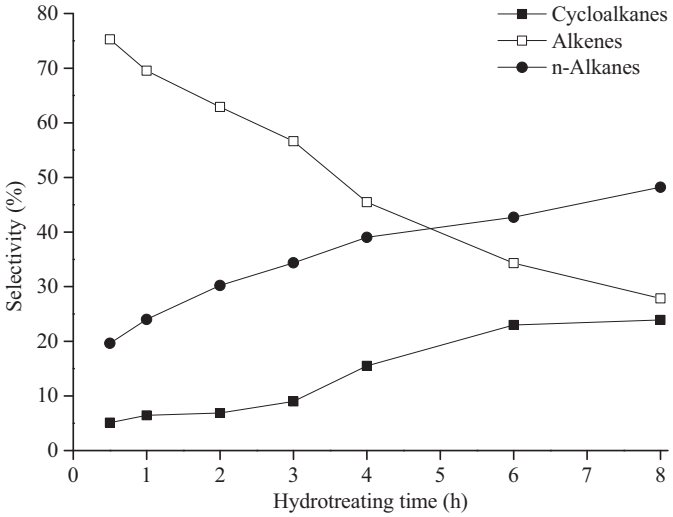

Fig. 15. Selectivity of different type of hydrocarbons (375 °C).

Hydrocracking and polymerization are also observed, which are verified by the diversified hydrocarbons in the final liquid products (Figs. 6 and 7). Hydrocracking degree (HCD) and polymerization degree (PMD) are defined as the number of C–C bond going through breakage and formation, respectively (Eqs. (13) and (14)). In the equations, the number of C–C bond breakage based on one unit weight is calculated as the ratio of moles of increased light molecules (carbon number lower than 17) to moles of cracked C_{17} and $C_{18}-1$. The actual mole of C–C breakage is the value multiplied by total hydrocracking conversion of C_{17-18} to C_{8-16}($x_{17,18\rightarrow 8-16}$); the PMD is calculated similarly. The obtained HCD and PMD are plotted in Fig. 14. It is shown that both values are increasing with reaction time, which indicates that hydrocracking and polymerization proceed throughout the entire reaction. Comparing the HCD and PMD, it is noticed that the hydrocracking is more intense than the polymerization.

$$\text{Hydrocracking degree(HCD)} = \left(\frac{\sum_i \Delta n_{i(i=8,9\ldots16)}}{\Delta HDC\,(n_{17}+n_{18})} - 1\right) \times x_{17,18\rightarrow 8-16} \tag{13}$$

$$\text{Polymerization degree(PMD)} = \left(\frac{\Delta PMD\,(n_{17}+n_{18})}{\sum_j \Delta n_{j(j=19,20\ldots30)}} - 1\right) \times x_{17,18\rightarrow 19-30} \tag{14}$$

Cyclization reaction is also observed through the formation of cycloalkanes. As seen from Fig. 15, the selectivity of cycloalkanes increases from 5 to 24% and *n*-alkane from 20 to 48% during the reaction, which compensates the decrease of selectivity of alkenes. The results suggest cyclization is more commonly from the isomerization of alkenes rather than de-hydrogenation of *n*-alkanes. The high accumulation of alkenes facilitates the cyclization reaction. It is worth noting that no aromatics are detected in the work, which indicates the reaction ceases at cycloalkanes without further de-hydrogenation.

3.4. Comparison of supported and unsupported catalysts

The supported Co/NiMoS with Al_2O_3 have been widely used in the industry and laboratory settings. With supports, catalysts demonstrate significant difference on hydrotreating performance and the kinetics can be altered. In this work, the hydrotreating

Table 3
Comparison of HDO/HDC product ratios on supported and unsupported catalysts.

Feed oils	Catalysts	Hydrotreating temperature (°C)	C_{18}/C_{17} ratio	HYD (%)	HC/PM (%)	ISO (%)
Methyl heptanoate [13]	$CoMoS/Al_2O_3$	250	1.7–2.0	14.1	–	–
	$NiMoS/Al_2O_3$	250	1.7–2.0	80.6	–	–
Rapeseed oil [33]	$NiMoS/Al_2O_3$	360	2.1	100	1.2/1.4	13.4
Sunflower oil [11]	$NiMoS/Al_2O_3$	300–450	1.0–2.3	100	2–22/–	4–12
Waste cooking oil [1]	$CoMoS/B_2O_3–Al_2O_3$	350	1.5–3.0	–	–	–
	$NiMoS/B_2O_3–Al_2O_3$	350	1.5–4.0	99.0	4.3*	7.5
Waste cooking oil	Unsupported CoMoS	375	0.6	65.0	11.1/7.9	<0.1

Hydrogenation: HYD = alkanes/(alkenes + alkanes) × 100%.
Hydrocracking: HC = cracked hydrocarbons/total hydrocarbons × 100%.
Polymerization: PM = polymerized hydrocarbons/total hydrocarbons × 100%.
Isomerization: ISO = branched hydrocarbons/total hydrocarbons × 100%.
* Sum of HC and PM.

results with unsupported CoMoS are compared to other researches with supported catalysts. The product distribution shows that an unsupported catalyst has a significant lower C_{18}/C_{17} ratio (0.6) than that of supported catalysts (Table 3). Mathematically, the lower C_{18}/C_{17} may be attributed to either the decrease of C_{18} or the increase of C_{17}. However, there is lack of evidence to support the hypothesis that unsupported catalyst tends to promote the decarbonation process. Our results show that the decarbonation is mainly occurring on the sulfur saturated active sites on Co–Mo catalysts and it suffers from catalyst deactivation. The discussion may indicate that production of C_{18} is low over unsupported catalyst due to lack of acidity. This is consistent with the research by Ryymin et al. that large amount of Lewis acid sites on Al_2O_3 supports can benefit the hydrogenation and dehydration reactions [16]. In addition, comparing to supported catalysts, higher hydrocracking and polymerization are noticed when dealing with unsupported catalysts [1,34], indicated by HC and PM values (Table 3). Lack of acidic support, lower hydrocracking is expected to obtain. The higher C–C breakage and formation may be due to the high reaction temperature. Therefore, a support with Lewis acid sites may play an important role in the selectivity for the hydrodeoxygenation pathways and promoting the final product quality.

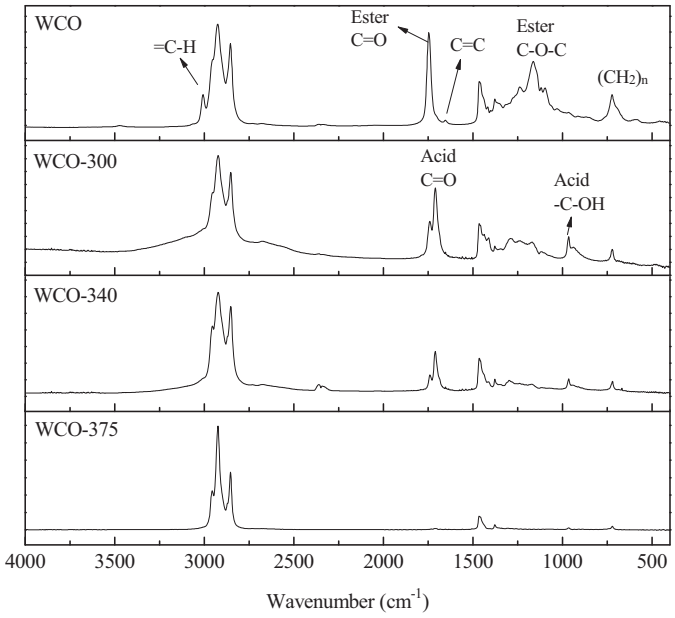

Fig. 16. FTIR spectra of original and hydrotreated WCO (8 h).

3.5. Temperature effect on reaction degree

Temperature is an important factor influencing the overall reaction rate. In this study, experiments were conducted at three different temperatures, 300, 340 and 375 °C. The FTIR spectra for original and hydrotreated WCO are shown in Fig. 16. At the lowest temperature of 300 °C, the main products are mono-/di-glycerides and carboxylic acid converted from triglyceride, as evidenced by large characteristic peaks of ester and fatty acid at 1742 and 1711 cm^{-1}. A brown wax, as oppose to a liquid product, is produced when the reactor is cooled down to room temperature (20 °C). Propane and propene are detected in gas phase, which is obtained from the hydrotreating of the resultant glycerol through de-esterification (Fig. 10). At the highest temperature, 375 °C, triglycerides in WCO are almost fully converted into hydrocarbons. The characteristic peaks of esters at 1742 and 1170 cm^{-1} disappear, only the peaks standing for C–H bond in alkanes are observed. The main product is alkanes and alkenes with tiny amount fatty acid (<1%).

Gas chromatography and elemental analysis are used to determine the product distributions and oxygen conversion rate at all three temperatures (Fig. 17). At 300 °C, 67.6% of glycerides are consumed to form fatty acids with 14% hydrocarbons generated, which implies that the deoxygenation from fatty acids is the rate limiting step and degradation of triglycerides is the predominant reaction at this temperature. When increasing temperature to 340 °C, hydrodeoxygenation and hydrodecarbonylation/decarboxylation take place to a larger extent, indicated from the dramatic increase of oxygen conversion. At 375 °C, the oxygen conversion is approaching 100%, which indicates the hydrocarbon is generated quickly compared to the lower temperatures. However, lower diesel yields are obtained at higher temperature. The yield of $C_{15–18}$ upon total hydrocarbon is 81% for 375 °C, comparing to 94.6% and 94.1% for

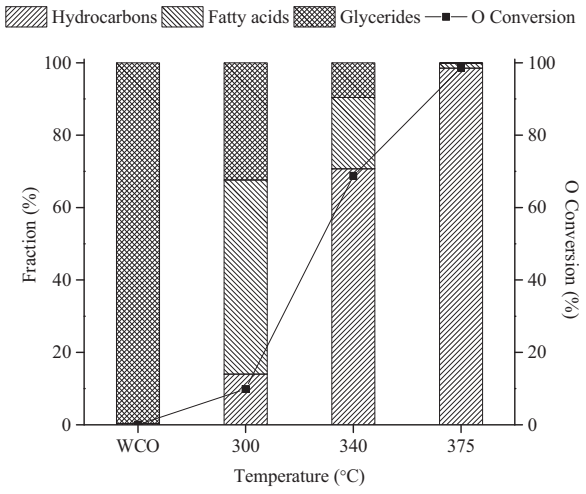

Fig. 17. Temperature effect on product distribution (8 h).

Table 4
Properties and hydrocarbon distribution of original and hydrotreated WCO at different temperatures (8 h).

	WCO	WCO-300	WCO-340	WCO-375
Density (g/ml)@30 °C	0.9184	0.8935	0.8661	0.8138
C_{18}/C_{17} mass ratio	–	0.70	0.64	0.62
C_{15-18} selectivity (%)	–	94.6	94.1	81.0
Paraffin selectivity (%)	–	18.5	38.4	65.0
H/C atomic ratio	1.81	1.93	1.98	2.04

Table 5
Estimated parameters at different temperatures.

Parameters	WCO-300	WCO-340	WCO-375
k_1	0.3007 ± 0.0128	1.5628 ± 0.0602	6.0672 ± 0.2173
k_2	0.0265 ± 0.0021	0.1032 ± 0.0074	0.2123 ± 0.0112
k_3	0.0753 ± 0.0057	0.3011 ± 0.0203	0.6376 ± 0.0231

300 and 340 °C, respectively (Table 4). Increased paraffin selectivity and H/C atomic ratio also indicate that temperature can facilitate hydrogenation reactions (Table 4).

Kinetic modeling for deoxygenation reactions at 300 and 340 °C was performed according to Scheme 1. The same reaction order and deactivation constants were assumed as 375 °C for better comparison. The estimated rate constants are shown in Table 5. For all three temperatures, the rate constant for decomposition of glycerides (k_1) is much higher than deoxygenation steps (k_2 and k_3), indicating deoxygenation is rate-limiting step for all the investigated temperatures. In addition, similar to 375 °C, HDC is also the dominate deoxygenation route at 300 and 340 °C, as seen from the larger k_3. With increase in reaction temperature, all the rate constants are increased. The rate constant for HDO pathway (k_2) increases by a factor of 8.0 from 300 to 375 °C, whereas the rate constant for HDC route (k_3) increases by a slightly higher factor of 8.5 in the same temperature range. This indicates the effect of temperature is similar on HDO and HDC pathways over this unsupported CoMoS, and HDC is slightly more favorable at higher temperature.

4. Conclusions

Hydrodeoxygenation of waste cooking oil on unsupported CoMoS catalysts was investigated in a batch reactor. Analysis of WCO and hydrotreated products shows that the oxygen containing compounds (glycerides) are mainly converted to C_{17} and C_{18} hydrocarbons, while acids, aldehydes and alcohols are identified as major intermediates. Accompanying the deoxygenation reaction, side reactions, such as hydrogenation, hydrocracking, polymerization, and cyclization are also taking place.

Reaction schemes are proposed on the deoxygenation process according to the kinetic modeling results. The estimation indicates that the total HDC reaction routes (hydro decarbonylation and decarboxylation) are the predominant pathways to eliminate oxygen, with the rate constant three times as high as HDO. Direct hydrodecarbonylation from fatty acids is the main HDC reaction route with the highest rate constant. HDO consists of a series of reactions, transferring fatty acids to aldehydes/alcohols and then to final C_{18} hydrocarbon products. Direct reduction to alcohols from fatty acids is dominant over the pathway from fatty acids to aldehydes, suggesting alcohols are the more important intermediates than aldehydes for the HDO process. The higher dehydration rate constant indicates that the reduction of fatty acids is the rate limiting step. From a finalized scheme, three main reaction pathways are determined and the order of their rate constants from high to low is decarbonylation of fatty acid, hydrodeoxygenation to produce alcohols, and decarboxylation of fatty acids.

Selective deactivation is observed on the HDC route, with 80% of activity lost in 8 h, while HDO maintains the initial activity during the whole reaction process. The lost catalyst activity is attributed to the gradual loss of sulfur from the catalyst surface. It indicates that HDC is mainly occurring on saturated sites, which is highly related to the sulfur coverage, and HDO happens on the sulfur vacancies.

Based on the product distribution, side reactions of hydrogenation, hydrocracking, polymerization, and cyclization occur continuously along the reaction. Analyzing the results shows that hydrogenation is more intense in the first half an hour since the total number of double bonds decreases dramatically from 2.1 to 1.5. Hydrocracking is more intense than the polymerization as the degree of hydrocracking is six times that of polymerization at 8 h. Cyclization is more commonly developed from the isomerization of alkenes as oppose to the de-hydrogenation of *n*-alkanes.

Temperature is another key factor for the reaction rate. At low temperature 300 °C, the main products are mono-/di-glycerides and carboxylic acids, which indicates insufficient hydrodeoxygenation. At high temperature 375 °C, fatty acid triglycerides in WCO are almost fully converted into hydrocarbons but with lower diesel selectivity due to a higher hydrocracking and polymerization.

Acknowledgement

The authors gratefully acknowledge the financial assistance from Natural Sciences and Engineering Research Council of Canada, Canada Foundation for Innovation and Atlantic Canada Opportunities Agency.

References

[1] M. Toba, Y. Abe, H. Kuramochi, M. Osako, T. Mochizuki, Y. Yoshimura, Catal. Today 164 (2011) 533–537.
[2] S. Bezergianni, A. Kalogianni, A. Dimitriadis, Fuel 93 (2012) 638–641.
[3] S. Bezergianni, A. Kalogianni, Bioresour. Technol. 100 (2009) 3927–3932.
[4] T. Kalnes, T. Marker, D.R. Shonnard, Int. J. Chem. Reactor Eng. 5 (2007) A48.
[5] B. Donnis, R.G. Egeberg, P. Blom, K.G. Knudsen, Top. Catal. 52 (2009) 229–240.
[6] I. Sebos, A. Matsoukas, V. Apostolopoulos, N. Papayannakos, Fuel 88 (2009) 145–149.
[7] J. Holmgren, C. Gosling, R. Marinangeli, T. Marker, G. Faracii, C. Perego, Hydrocarbon Process., Int. Ed. 86 (2007) 67–72.
[8] T.V. Choudhary, C.B. Phillips, Appl. Catal., A 397 (2011) 1–12.
[9] M. Krar, S. Kovacs, D. Kallo, J. Hancsok, Bioresour. Technol. 101 (2010) 9287–9293.
[10] J. Gusmão, D. Brodzki, G. Djéga-Mariadassou, R. Frety, Catal. Today 5 (1989) 533–544.
[11] G.W. Huber, P. O'Connor, A. Corma, Appl. Catal., A 329 (2007) 120–129.
[12] D. Kubicka, L. Kaluza, Appl. Catal., A 372 (2010) 199–208.
[13] O.I. Senol, E.M. Ryymin, T.R. Viljava, A.O.I. Krause, J. Mol. Catal. A: Chem. 268 (2007) 1–8.
[14] O.I. Senol, T.R. Viljava, A.O.I. Krause, Catal. Today 100 (2005) 331–335.
[15] E.M. Ryymin, M.L. Honkela, T.R. Viljava, A.O.I. Krause, Appl. Catal., A 358 (2009) 42–48.
[16] E.M. Ryymin, M.L. Honkela, T.R. Viljava, A.O.I. Krause, Appl. Catal., A 389 (2010) 114–121.
[17] A. Centeno, E. Laurent, B. Delmon, J. Catal. 154 (1995) 288–298.
[18] N.B. Van, D. Laurenti, P. Afanasiev, C. Geantet, Appl. Catal., B 101 (2011) 239–245.
[19] H.P. Zhang, H.F. Lin, Y. Zheng, Highly dispersed nanocrystalline molybdenum sulfide prepared by hydrothermal synthesis as an unsupported odel catalyst for ultra clean diesel, in: 21st Canadian Symposium on Catalysis, Banff, AB, 2010.
[20] M. Snare, I. Kubickova, P. Maki-Arvela, K. Eranen, J. Warna, D.Y. Murzin, Chem. Eng. J. 134 (2007) 29–34.
[21] P. Simacek, D. Kubicka, G. Sebor, M. Pospisil, Fuel 88 (2009) 456–460.
[22] R.B. Costa, d.A. Zellner, M.L. Crupi, M.R. De Fina, M.R. Valentino, P. Dugo, G. Dugo, L. Mondello, Flavour Fragance J. 23 (2008) 40–48.
[23] R.R. Chianelli, Catal. Rev. Sci. Eng. 26 (1984) 361–393.
[24] S. Harris, R.R. Chianelli, J. Catal. 98 (1986) 17–31.
[25] G. Vigli, A. Philippidis, A. Spyros, P. Dais, J. Agric. Food. Chem. 51 (2003) 5715–5722.
[26] A.S. Berenblyum, T.A. Podoplelova, E.A. Katsman, R.S. Shamsiev, V.Y. Danyushevsky, Kinet. Catal. 53 (2012) 595–609.
[27] D. Kubicka, J. Horacek, Appl. Catal., A 394 (2011) 9–17.
[28] L. Boda, O. Gyorgy, H. Solt, L. Ferenc, J. Valyon, A. Thernesz, Appl. Catal., A 374 (2010) 158–169.

[29] M.R. de Brimont, C. Dupont, A. Daudin, C. Geantet, P. Raybaud, J. Catal. 286 (2012) 153–164.
[30] C. Dupont, R. Lemeur, A. Daudin, P. Raybaud, J. Catal. 279 (2011) 276–286.
[31] J.G. Immer, H.H. Lamb, Energy Fuels 24 (2010) 5291–5299.
[32] H.G. Manyar, C. Paun, R. Pilus, D.W. Rooney, J.M. Thompson, C. Hardacre, Chem. Commun. 46 (2010) 6279–6281.
[33] L.D. Field, S. Sternhell, J.R. Kalman (Eds.), Organic Structures from Spectra Fourth, John Wiley& Sons Ltd, West Sussex, England, 2008.
[34] P. Simacek, D. Kubicka, G. Sebor, M. Pospisil, Fuel 89 (2010) 611–615.